A series of polyoxometalate compounds: syntheses, characterization, electrochemical sensing and photocatalytic properties

Yuan Gong[a], Tao Liu[b], Aixiang Tian[a,*], Jun Ying[a], Mengle Yang[a,*]

Experimental

Materials and General Methods

In the synthetic process, all reagents and solvents used are purchased from commercial sources and can be used without further purification (analytical purity, jiuding chemical (Shanghai) Co., Ltd.). The FT-IR spectra were recorded on the Magna FT-IR 560 spectrometer (KBr particles) with a measuring range of 4000-400 cm^{-1} (Thermo Fisher Nicolet, Waltham, MA, USA). The powder X-rays diffraction were tested on Ultima IV with a D/teX ultra-diffractometer (Rigaku Corporation, Japan). The solid-state diffuse-reflectance UV-Vis spectra record powder sample were on a PerkinElmer Lambda 750 UV-vis spectrometer equipped with an integrating sphere. UV-vis absorption spectra were obtained using a UV-1801 ultra violet spectrophotometer. The electrochemical measurement was carried out by CHI-660 electrochemical workstation (Shanghai Chenhua Instrument Co., Ltd.). The traditional three-electrode system was used, Ag/AgCl electrode as the reference electrode, platinum wire as the counter electrode and compound modified glassy carbon electrode (GCEs) as working electrode.

Preparation of compounds 1-4

Synthesis of $[Co_2(TPTP)_4(H_2O)_4(SiMo_{12}O_{40})]\cdot 4H_2O$ (1)

At room temperature, a mixture of $CoSO_4\cdot 7H_2O$ (0.1 g, 0.36 mmol), $(NH_4)_6Mo_7O_{24}\cdot 4H_2O$ (0.1 g, 0.08 mmol), $Na_2SiO_3\cdot 9H_2O$ (0.1g, 0.35 mmol) and TPTP (0.02 g, 0.048 mmol) was dissolved in 10 mL H_2O. pH of the mixture was adjusted to about 3.8 by the addition of 0.1 M HCl solution. Then, the suspension was transferred to a 20 mL Teflon-lined autoclave and kept at 150 °C for 5 days. After slow cooling to room temperature, orange block crystals of **1** was isolated and washed with distilled water (yields 30% based on Mo). Analytical and computational for **1** $C_{52}H_{80}Co_2Mo_{12}N_{16}O_{52}Si$ (3058.5001): C, 20.42; H, 2.63, N, 7.33%. Found: C, 20.32, H, 2.57, N, 7.40%.

Synthesis of $[Ni_2(TPTP)_4(H_2O)_4(SiMo_{12}O_{40})]\cdot 2.5H_2O$ (2)

At room temperature, a mixture of $NiSO_4\cdot 7H_2O$ (0.1 g, 0.38 mmol), $(NH_4)_6Mo_7O_{24}\cdot 4H_2O$ (0.1 g, 0.08 mmol), $Na_2SiO_3\cdot 9H_2O$ (0.1g, 0.35 mmol) and TPTP (0.02 g, 0.048 mmol) was dissolved in 10 mL H_2O. pH of the mixture was adjusted to about 3.7 by the addition of 0.1 M HCl solution. Then, the suspension was transferred to a 20 mL Teflon-lined autoclave and kept at 150 °C for 5 days. After slow cooling to room temperature, light green block crystals

of **2** was isolated and washed with distilled water (yields 33% based on Mo). Analytical and computational for **2** $C_{52}H_{77}Mo_{12}N_{16}Ni_2O_{50.5}Si$ (3030.9976): C, 20.60; H, 2.56, N, 7.39%. Found: C, 20.53, H, 2.51, N, 7.45%.

Synthesis of $\{[Cu(H_2TPTP)(TPTP)(H_2O)_3]_2(SiMo_{12}O_{40})_2\}\cdot 7.5H_2O$ (3)

At room temperature, a mixture of $CuSO_4\cdot 5H_2O$ (0.15 0.036), $(NH_4)_6Mo_7O_{24}\cdot 4H_2O$ (0.1 g, 0.08 mmol), $Na_2SiO_3\cdot 9H_2O$ (0.1g, 0.35 mmol) and TPTP (0.02 g, 0.048 mmol) was dissolved in 10 mL H_2O. pH of the mixture was adjusted to about 3.9 by the addition of 0.1 M HCl solution. Then, the suspension was transferred to a 20 mL Teflon-lined autoclave and kept at 150 °C for 5 days. After slow cooling to room temperature, green block crystals of **3** was isolated and washed with distilled water (yields 34% based on Mo). Analytical and computational for **3** $C_{52}H_{95}Cu_2Mo_{24}N_{16}O_{97.5}Si_2$ (4990.1813): C, 12.51; H, 1.92, N, 4.49%. Found: C, 12.45, H, 1.83, N, 4.53%.

Synthesis of $\{Cu_2(TPTP)_2(\beta\text{-}Mo_8O_{26})_{1/2}\}\cdot H_2O$ (4)

At room temperature, a mixture of $CuSO_4\cdot 5H_2O$ (0.15 0.036), MoO_3 (0.1 g, 0.69 mmol) and TPTP (0.02 g, 0.048 mmol) was dissolved in 10 mL H_2O. pH of the mixture was adjusted to about 3.8 by the addition of 0.1 M HNO_3 solution. Then, the suspension was transferred to a 20 mL Teflon-lined autoclave and kept at 150 °C for 6 days. After slow cooling to room temperature, yellow block crystals of **4** was isolated and washed with distilled water (yields 29% based on Mo). Analytical and computational for **4** $C_{26}H_{34}Cu_2Mo_4N_8O_{16}$ (1225.4445): C, 25.48; H, 2.80, N, 9.14%. Found: C, 25.41, H, 2.72, N, 9.17%.

Preparation of the glassy carbon electrode

First, the crystal and acetylene were weighed (5 mg) and then ground in mortar for 30 minutes to obtain a mixture. Adding 0.5 mL of distilled water and 10 ml of naphthalene benzene solution to the 4 mg mixture to form a suspension for 0.5 h by ultrasonic wave. Then we dropped the mixture onto the surface of a glass carbon electrode. After drying at room temperature for 1 h, 3 mL of naphthalene solution was dripped. Glassy carbon electrodes of **1**, **3**, and **4** (**1**–GCE, **3**–GCE, **4**–GCE) were obtained.

Photocurrent measurements

Firstly, the indium tin oxide (ITO) glass was ultrasonically washed in ethanol solution for 30 minutes, then cleaned with deionized water and dried. We added 10 mg of crystal powder to 0.4 ml of 0.5% Nafion isopropanol solution. After 1 h of ultrasonic mixing, we dropped the mixed solution onto ITO glass with a size of 10 × 10 mm^{-2}, and then dried the prepared working electrode at 60 °C for 4 h. An Ag/AgCl electrode was used as the reference electrode, platinum wire as the counter electrode, 0.5 M Na_2SO_4 aqueous solution was used as the supporting electrolyte, and the Xe lamp was used as the light source.

X-ray crystallographic study

X-ray diffraction analysis data was collected by using Bruker SMART APEX II with Mo-Kα radiation (λ = 0.71073 Å). All the structures were solved by the direct method, and the SHELXS-14 package was used to refine on F^2 by the full-matrix least squares method. The structures refinement and crystals data of **1**–**4** are shown in Table S1. The selected bond

angles and bond lengths of compounds **1**–**4** are summarized in Table S2. The CCDC numbers are 2339272, 2339289, 2348865, and 2339291 for **1**–**4** (Cambridge Crystal-lographic Data Center).

Table S1. Crystal data and structure refinement for compounds **1**–**4**.

Compounds	**1**	**2**	**3**	**4**
Formula	$C_{52}H_{80}Co_2Mo_{12}N_{16}O_{52}SiC_{52}H_{77}Mo_{12}N_{16}Ni_2O_{50.5}SiC_{52}H_{95}Cu_2Mo_{24}N_{16}O_{97.5}Si_2C_{26}H_{34}Cu_2Mo_4N_8O_{16}$			
*F*w	3058.55	3031.08	4990.25	1225.45
Crystal system	monoclinic	monoclinic	triclinic	triclinic
Space group	$P2_1/c$	$P2_1/n$	P-1	P-1
a/(Å)	12.5361(6)	12.5205(4)	12.5392(3)	12.7451(7)
b/(Å)	15.4564(7)	15.3929(6)	13.1412(3)	12.7628(8)
c/(Å)	23.5236(12)	23.5897(8)	21.0778(5)	13.4678(7)
α/(°)	90	90	89.2190(10)	95.939(2)
β/(°)	92.0090(10)	91.9870(10)	83.5790(10)	109.007(2)
γ/(°)	90	90	62.0770	112.422(2)
Volume/(Å^3)	4555.2(4)	4543.6(3)	3046.631(13)	1848.57(18)
Z	2	2	1	2
D_c (g·cm^{-3})	2.230	2.216	2.718	2.202
μ(mm^{-1})	2.063	2.115	2.859	2.527
F(000)	2948.0	2958.0	2393.0	1200.0
R1[a] [I > 2σ(I)]	0.0407	0.0320	0.0680	0.0452
wR_2[b] (all data)	0.0937	0.0761	0.1450	0.1146
GOF on F^2	1.045	1.106	1.139	1.033

[a] $R_1=\sum\|F_o\|-|F_c\|/\sum|F_o|$. [b] $wR_2=\{\sum[w(F_o^2-F_c^2)^2]/\sum[w(F_o^2)^2]\}^{1/2}$

Table S2. Selected bond lengths (Å) and angles (°) of compounds **1**–**4**.

Compound **1**			
Co (1) – O3W	2.077(4)	Co (1) – O4W	2.107(4)
Co (1) – N (4)	2.119(5)	Co (1) – N (1)^{2}	2.180(5)
O3W – Co (1) – O4W	85.10(19)	O4W– Co (1) –N (1)^{2}	95.47(18)
N (4)– Co (1) – N (1)^{2}	97.46(2)	O3W – Co (1) – N (1)^{2}	87.18(18)
N (4)– Co (1) – N (8)^{3}	84.40(18)	O3W – Co (1) – N (4)	90.24(18)
Symmetry codes: ^{1}1-X,2-Y,1-Z; ^{2}3/2-X,1/2+Y,3/2-Z; ^{3}1/2-X, -1/2+Y,3/2-Z			
Compound **2**			
Ni (1) – O1W	2.073(3)	Ni (1) – O4W	2.062(3)
Ni (1) – N (4)	2.090(3)	Ni (1) – N (3)	2.050(3)
N (1) – C (20)	1.326(6)	N (3) – N (7)	1.382(5)
N (1) – C (26)	1.330(6)	N (3) – C (10)	1.306(5)
C (20)– N (1) – Ni (1)^{4}	121.0(3)	N (6)– N (4) – Ni (1)	121.4(2)
C (10)– N (3) – Ni (1)	129.2(3)	C (12)– N (8) – Ni (1)^{5}	118.1(3)
Symmetry codes: ^{1}1-X, -Y,1-Z; ^{2}1/2-X,1/2+Y,1/2-Z; ^{3}3/2-X,-1/2+Y,1/2-Z			
Compound **3**			
Cu(1) – N(4)	1.960(9)	Cu(1) – O2W	1.937(9)
Cu(1) – O1W	2.263(11)	Cu(1) – O3W	1.950(11)
O3W– Cu(1) – O1W	96.2(6)	O2W – Cu(1) –O1W	90.1(5)
O2W– Cu(1) – N(8)	173.3(4)	O3W – Cu(1) – N(4)	170.9(5)
N(4) – Cu(1) – O1W	91.4(5)	N(4)– Cu(1) – N(8)	95.0(4)
Symmetry codes: ^{1}2-X,1-Y,1-Z; ^{2}-X,2-Y,2-Z			
Compound **4**			
Cu (1) – N (1)^{2}	2.031(5)	Mo (2)-O (14)	1.702(4)
Cu (1) – N (8)^{3}	2.004(5)	Cu (1) – O (14)	2.239(4)
Cu (1) – N (7)	1.988(4)	Cu (2) – N (6)	1.966(5)
Cu (2) – N (5)^{4}	2.006(5)	Cu (2) – N (3)	1.970(5)
N (7)-Cu (1)-N (1)^{2}	120.94(18)	N (8)^{3}-Cu (1)-N (1)^{2}	110.80(18)
N (6)-Cu (2)-N (5)^{4}	114.1(2)	N (3)-Cu (2)-N (5)^{4}	120.7(2)
N 1)^{2}-Cu (1)-O (14)	85.94(17)	N (8)^{3}-Cu (1)-O (14)	96.26(18)
Mo (2)-O (14)-Cu (1)	142.2(2)	N (8)-N (5)-Cu (2)^{4}	120.4(4)
Symmetry codes: ^{1}3-X, 2-Y, 1-Z; ^{2}2-X, 1-Y, 1-Z; ^{3}+X, 1+Y, -1+Z; ^{4}2-X, -Y, 2-Z			

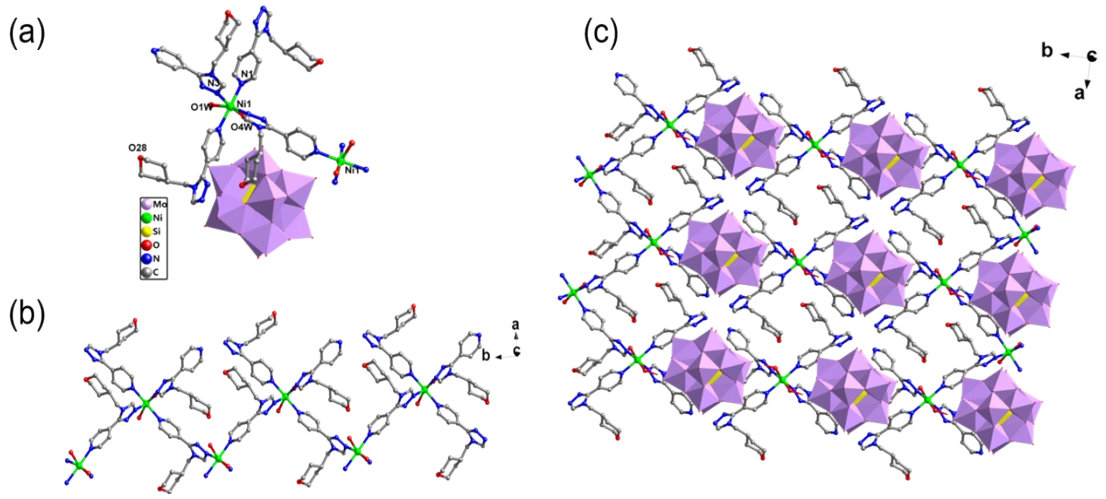

Fig. S1 (a) Polyhedral/ball/stick view of the unit of **2**. The hydrogen atoms and free water molecules are omitted for clarity. (b) A 1D grid-like metal-organic layer (c) The 2D supramolecular layer of **2**.

Compounds **1**–**4** were characterized by FT-IR spectroscopy (Fig. S2). The characteristic peaks at 645–965 cm^{-1} for **1**, 637–995 cm^{-1} for **2**, 624–960 cm^{-1} for **3** belong to υ(Si–O_a), υ(Mo–O_t) and υ(Mo–$O_{b/c}$–Mo). The characteristic peaks at 555–954 cm^{-1} for **4** belong to υ(Mo-O_t) and υ(Mo-$O_{b/c}$-Mo). The characteristic peaks in the region of 1066–1617 cm^{-1} for **1**, 1096–1623 cm^{-1} for **2**, 1071–1659 cm^{-1} for **3**, and 1085–1624 cm^{-1} for **4** are ascribed to the ligand TPTP.

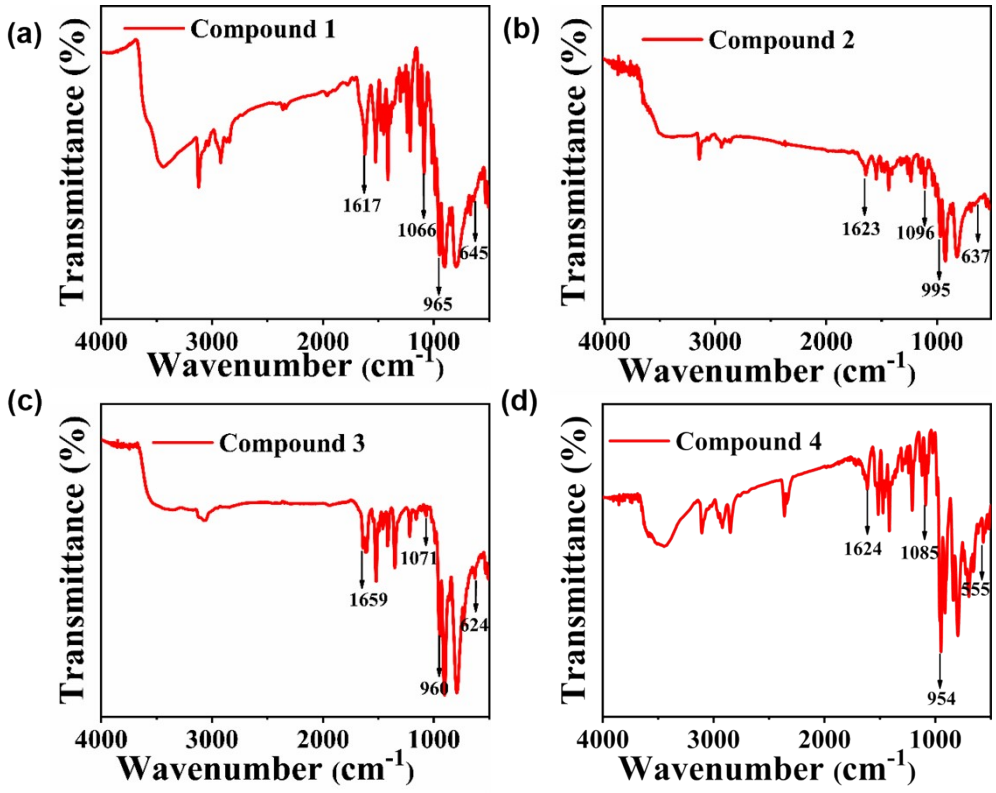

Fig. S2. The IR spectra of compounds **1**–**4**.

The crystal purity of compounds **1**–**4** was determined by PXRD. The good agreement with the simulated diffraction peaks shows the crystal phase purity of compounds **1**–**4** (Fig. S3).

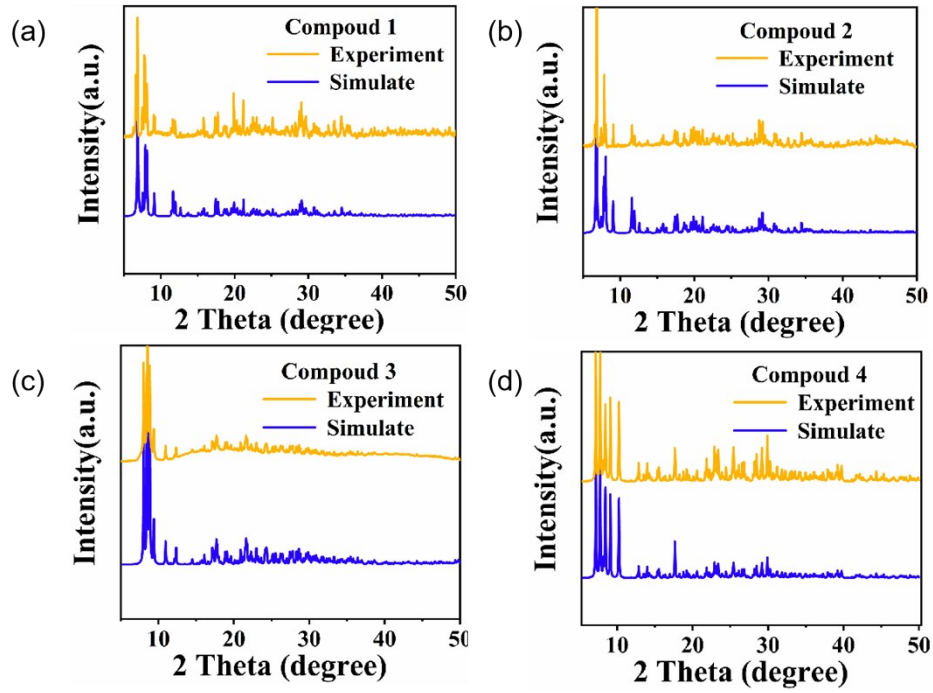

Fig. S3. The PXRD patterns of compounds **1**–**4.**

we have tested the stability of compounds in different organic solvents. The results show that the compounds remain stable in different organic solvents (Fig. S4).

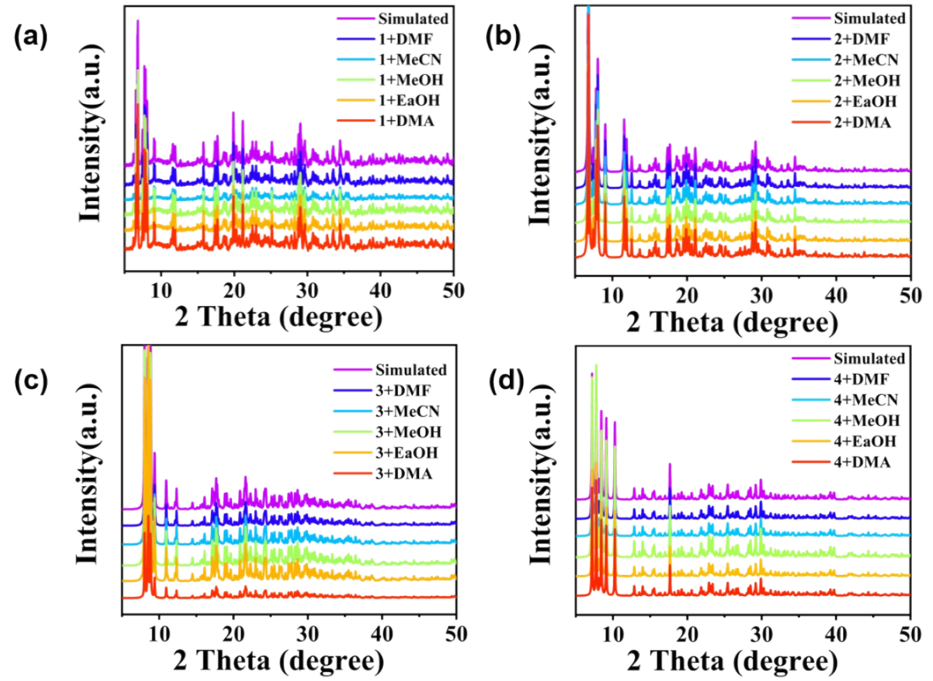

Fig. S4. The PXRD patterns of compounds **1-4**.

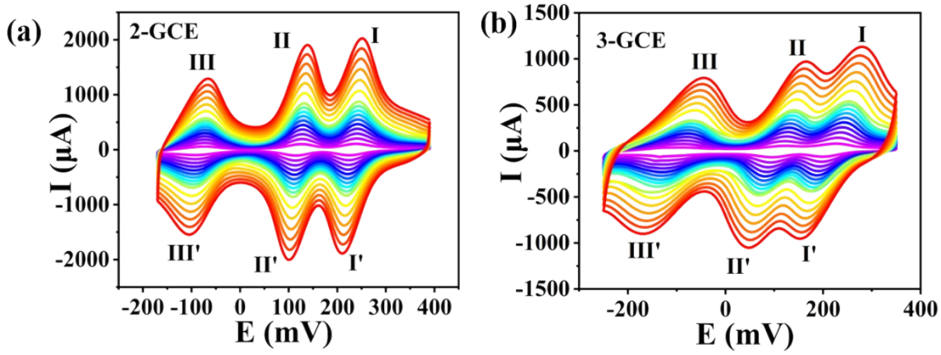

Fig. S5. The CV curves of **2**/**3**–GCE in electrolyte solution at a scanning rate of 20-500 mV s^{-1}.

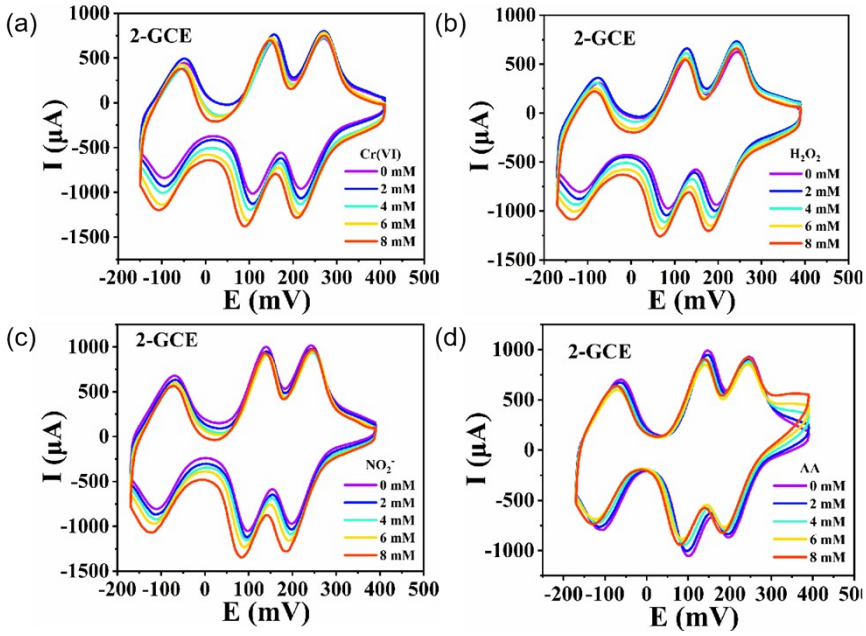

Fig. S6. (a-d) The CV curves of **2**–GCE in electrolyte solution containing 0-8 mM Cr(VI), H_2O_2, NO_2^-, and AA.

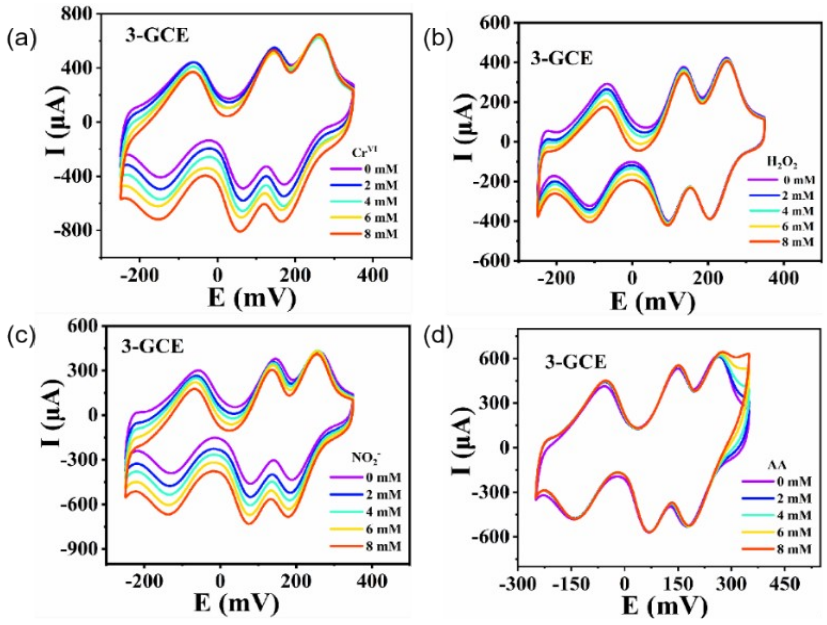

Fig. S7. (a-d) The CV curves of **3**–GCE in electrolyte solution containing 0-8 mM Cr(VI), H_2O_2, NO_2^-, and AA.

Compared with n-GCEs, the electrocatalytic performance of bare glassy carbon electrode on AA/Cr(VI)/KNO_2/H_2O_2 is negligible. The results show that bare–GCE in electrolyte solution has no electrocatalytic performance on Cr(VI), H_2O_2, NO_2^-, and AA (Fig. S8).

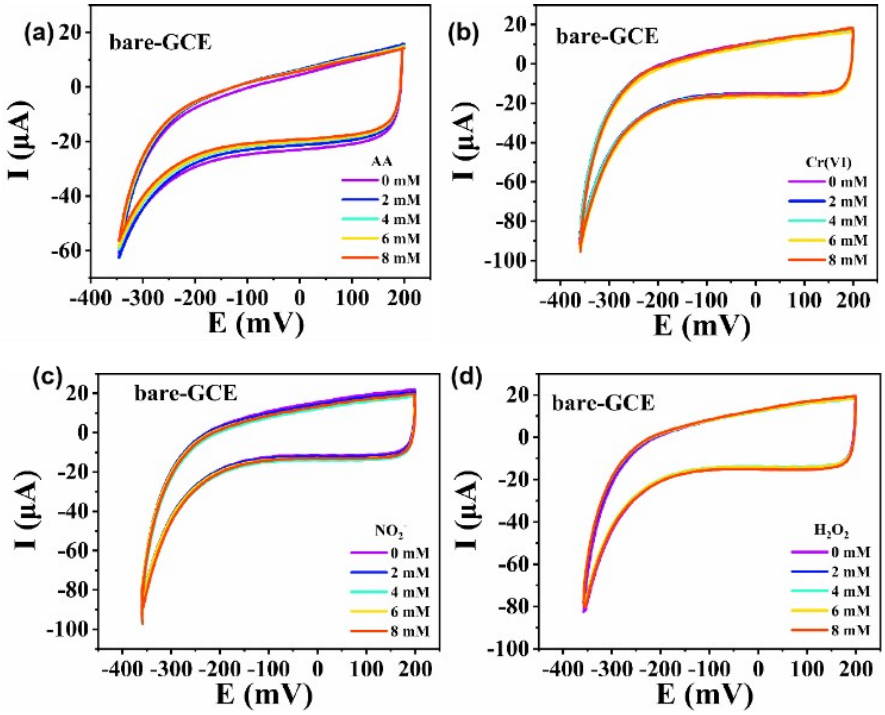

Fig. S8. (a-d) The CV curves of bare–GCE in electrolyte solution containing 0-8 mM Cr(VI), H_2O_2, NO_2^-, and AA.

Table S3. Amperometric sensor data of **1**– and **4**–GCE.

GCE	Test substance	Response time(s)	Concentration range(M)	Sensitivity (μA mM^{-1})	Correlation coefficient	Detection limit(M)
1–GCE	NO_2^-	2.7	3×10^{-6}–6.9×10^{-5}	4.30216	0.99738	6.2×10^{-2}
4–GCE	NO_2^-	3.6	3×10^{-6}–6.9×10^{-5}	5.0861	0.99288	1.17×10^{-2}
1–GCE	Cr(VI)	1.8	5×10^{-6}–1.1×10^{-4}	7.1	0.99608	1.6×10^{-2}
4–GCE	Cr(VI)	1.8	5×10^{-6}–1.15×10^{-4}	7.822	0.99574	1.9×10^{-2}

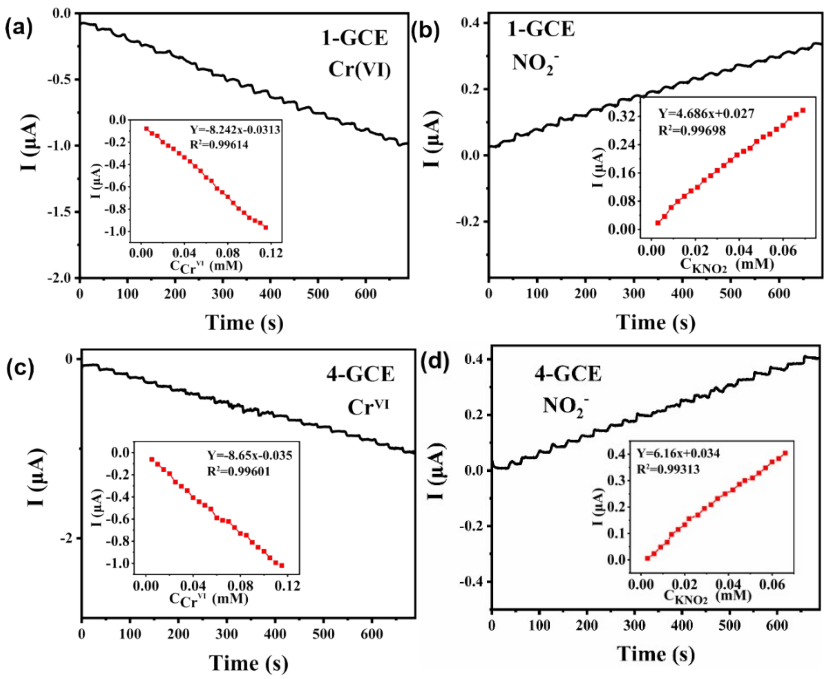

Fig. S9. Amperometric response for the **1**/**4**–GCEs for a week on successive addition of 0.1 mM nitrite and 0.1 mM Cr(VI) to electrolyte solution, respectively. The inset: the steady-state calibration curve for current.

Table S4. The analytical data for **1**/**4**–GCEs as amperometric sensors for a week.

CE	Test substance	Response time(s)	Concentration range(M)	Sensitivity (μA mM^{-1})	Correlation coefficient	Detection limit(M)
1–GCE	NO_2^-	4.5	3×10^{-6}–6.9×10^{-5}	4.686	0.99698	1.28×10^{-2}
4–GCE	NO_2^-	3.6	3×10^{-6}–6.9×10^{-5}	6.16	0.99313	9.79×10^{-3}
1–GCE	Cr(VI)	3.6	5×10^{-6}–1.1×10^{-4}	8.242	0.99614	1.46×10^{-2}
4–GCE	Cr(VI)	4.5	5×10^{-6}–1.1×10^{-4}	8.65	0.99601	1.38×10^{-2}

15.0 mg compounds **1** and **2** were added to the aqueous solution of 0.02 $mmol^{-1}$ MB/RhB (90 ml), respectively. Magnetic stirring was performed in the dark for 15 min and irradiated with an ultraviolet mercury lamp. The absorbance of the solution was measured by a UV-1801 ultraviolet spectrophotometer. The photocatalytic activities of these compounds in MB/RhB were determined.

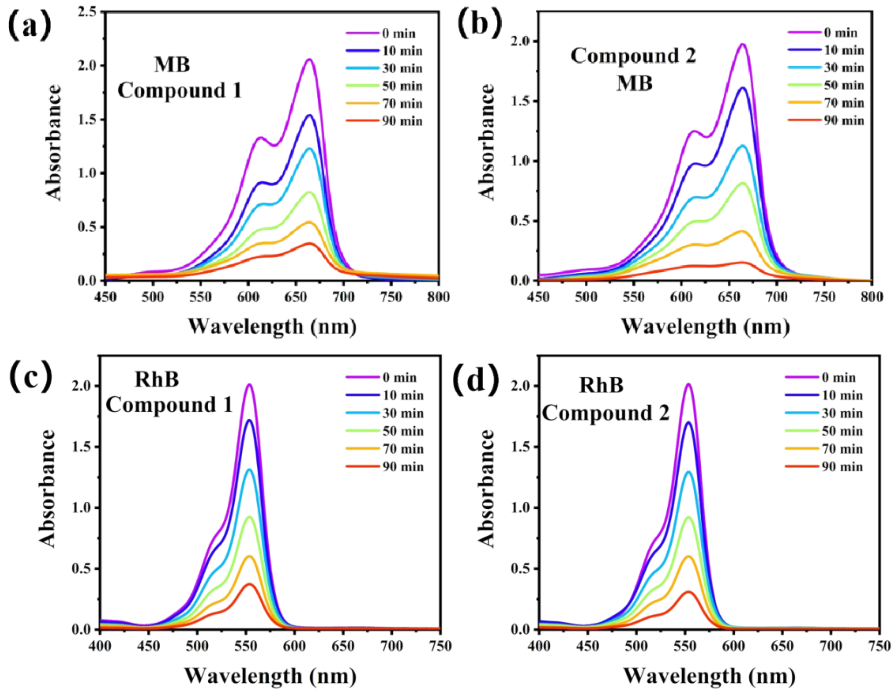

Fig. S10. (a-d）The absorption spectra of MB/RhB solution during the decomposition reaction under UV irradiation with compounds **1**–**2** as catalysts.

As shown in Fig. S11(a-b), within 90 min of UV irradiation, the photocatalytic degradation ratio of MB reached to 85.3% for **1**, 88% for **2**. The photocatalytic degradation ratio of RhB reached to 83% for **1**, 84.4% for **2**. As shown in Fig. S11(c-d), the catalytic activities of compounds **1** and **2** for photocatalytic degradation of MB/RhB hardly changed after four cycles.

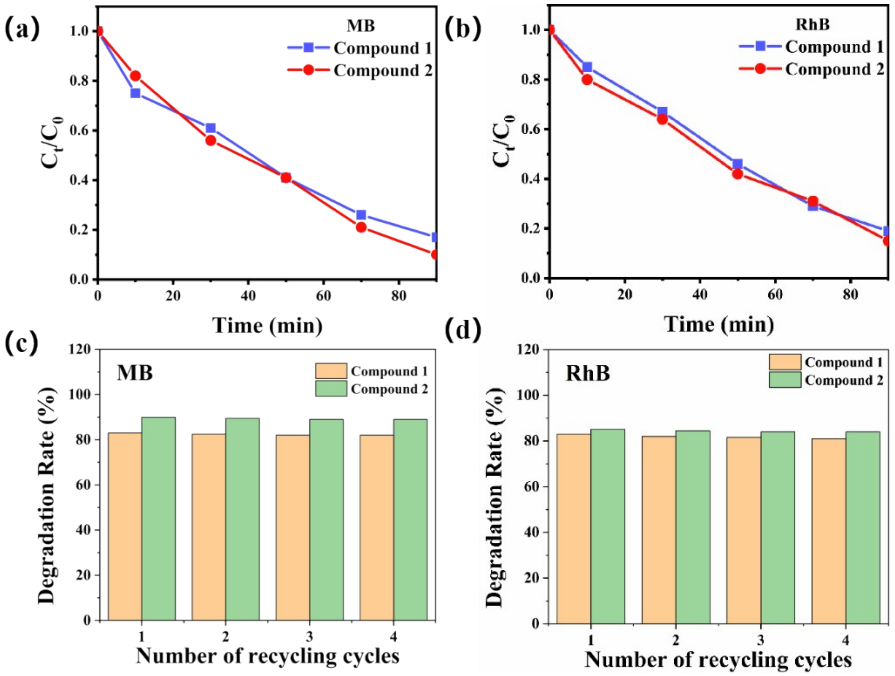

Fig. S11. (a-b) The catalytic conversion curves of compounds **1**–**2**. (c-d) Four cycles of photocatalytic degradation of compounds **1**–**2**.

The diffraction peak positions of the compounds before and after photocatalysis were in good agreement (Fig. S12), indicating that the compounds were stable before and after photocatalysis.

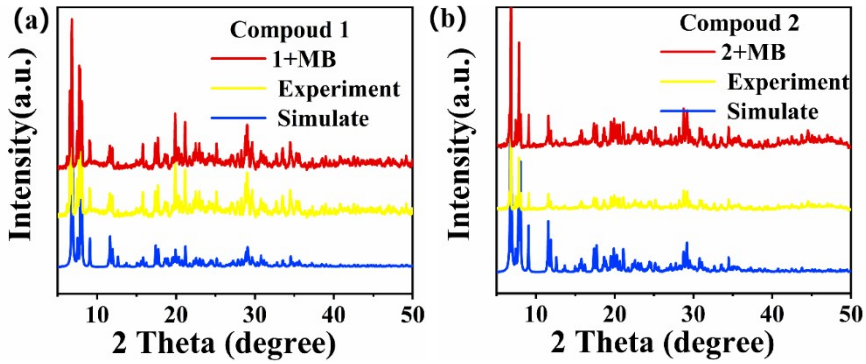

Fig. S12. PXRD of compounds **1** and **2** before and after photocatalysis.

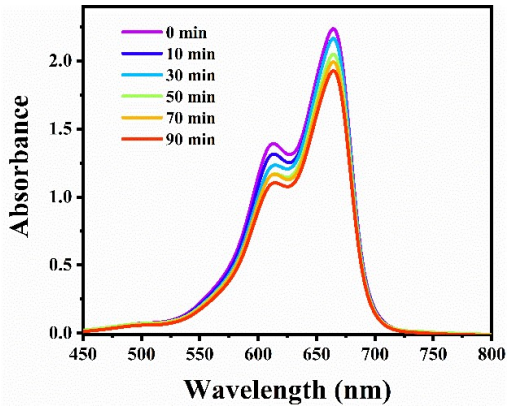

Fig. S13. The UV spectra of the MB solution without compounds used as the photoreduction catalysts.

Table S5. Comparison of the catalytic performance with other compounds for MB.

Catalyst(mg)	time	conversion	Ref.
1	90 min	85.3%	This work
2	90 min	88%	This work
1	120 min	57.3%	S1
1	120 min	52%	S2
6	120 min	59.6%	S3
1	90 min	79.8%	S4

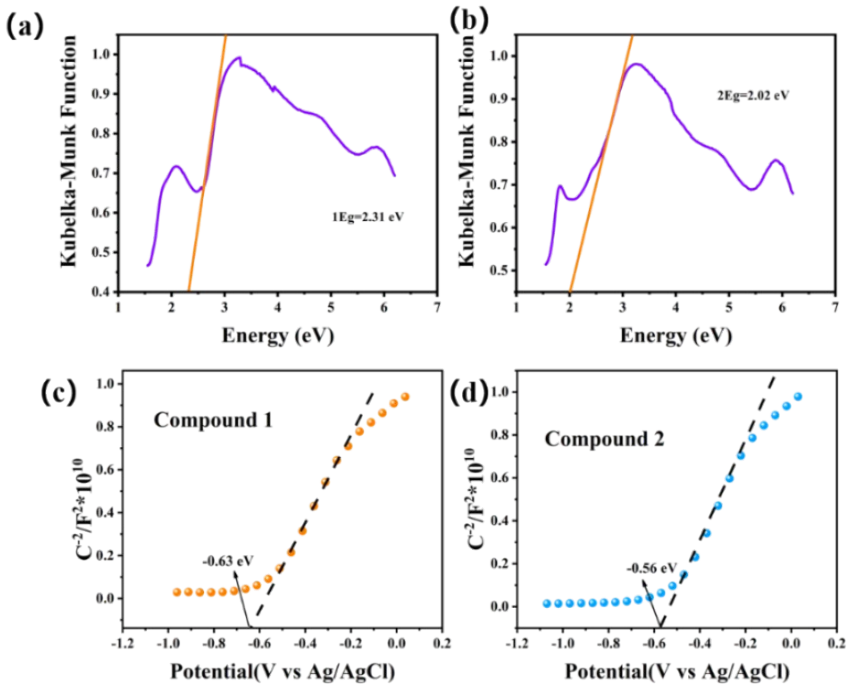

Fig. S14. (a, b) The optical band gap of compounds **1** and **2**. (c, d) Mott Schottky plot of compounds **1** and **2**.

[S1]. C. Wang, J. Ying; H. C. Mou, A. X. Tian, and X. L. Wang, *Inorg. Chem. Front.*, 2020, **7**, 3882.

[S2] S. F. Ma, J. Ying, Y. P. Zhang and A.X. Tian, *CrystEngComm*, 2022, **24**, 2891.

[S3] J. Ying, B. Y. Zhang, A. X. Tian and X.L. Wang, *CrystEngComm*, 2021, **23**, 2572.

[S4]. U. Khan, M. Akhtar, F. U. Khan, J. Peng, A. Hussain, H. F. Shi, J. Du, G. Yan, and Y. G. Li, *Journal of Coord. Chem.*, 2018, **71**, 16-18.